MethodsX 13 (2024) 102871

Contents lists available at ScienceDirect

MethodsX

journal homepage: www.elsevier.com/locate/methodsx

Automated image processing algorithm for 3D OCT images of fouling in spacer-filled membrane filtration channels ☆

Kees Theo Huisman [a,b,c,*], Luca Fortunato [a,d], Johannes S. Vrouwenvelder [a,b], Bastiaan Blankert [a]

[a] *Water Desalination and Reuse Center, Biological and Environmental Science and Engineering Division (BESE), King Abdullah University of Science and Technology (KAUST), Thuwal 23955-6900, Saudi Arabia*
[b] *Environmental Science and Engineering Program, Biological and Environmental Science & Engineering (BESE) Division, King Abdullah University of Science and Technology (KAUST), Thuwal 23955-6900, Saudi Arabia*
[c] *College of Science and Engineering, Hamad Bin Khalifa University, Qatar Foundation, Doha, Qatar*
[d] *MANN+HUMMEL Water & Fluid Solutions S.p.A., Italy*

ARTICLE INFO

Method name:
Merging of CT and OCT datasets

Keywords:
Optical coherence tomography
Automated image processing
3D reconstruction
Feed spacer
Spiral wound
Biofilm
Reverse osmosis

ABSTRACT

OCT imaging is an important technique to study fouling in spacer-filled channels of reverse osmosis systems for seawater desalination. However, OCT imaging of membrane filtration channels with feed spacers is challenging because the spacer material can be (partly) transparent, making it difficult to detect and possibly mistaken for fouling, and the longer optical pathway through the spacer material distorts the image below the spacer. This study presents an automated 3D OCT image processing method in MATLAB for visualization and quantification of biofouling in spacer-filled channels. First, a spacer template of arbitrary size and rotation was generated from a CT scan of the feed spacer. Second, background noise and file size were reduced by representing the OCT image with a list of discrete reflectors. Finally, the spacer template was overlayed with the feed spacer in the 3D OCT image, enabling automated visualization of the feed spacer and correction of the distortions. Moreover, the method allows the selection of datasets with the same location relative to the position of the spacer, enabling systematic comparison between datasets and quantitative analysis.

- A spacer template of arbitrary size and rotation was generated from a CT scan.
- The background noise was removed, and the file size was reduced by representing the OCT dataset with a list of discrete reflectors.
- The spacer template was overlayed with the feed spacer in the 3D OCT image.

Specifications table

Subject area:	Environmental Science
More specific subject area:	*Optical coherence tomography, Membrane filtration*
Name of your method:	*Merging of CT and OCT datasets*
Name and reference of original method:	*n/a*
Resource availability:	*MATLAB functions and instructions are provided in the supplementary material.*

☆ **Related research article:** K. T. Huisman, L. Fortunato, J. S. Vrouwenvelder, B. Blankert, A clear view of biofouling in spacer filled membrane filtration channels: Integrating OCT and CT for improved visualization and localization, Journal of Membrane Science, Volume 697, 2024, 122,573, ISSN 0376–7388, https://doi.org/10.1016/j.memsci.2024.122573.

* Corresponding author.
E-mail address: khuisman@hbku.edu.qa (K.T. Huisman).

https://doi.org/10.1016/j.mex.2024.102871
Received 23 February 2024; Accepted 18 July 2024
Available online 20 July 2024

Method details

Introduction

OCT imaging is a powerful tool that allows in-situ visualization of fouling in feed spacer-filled membrane filtration channels [1,2]. Feed spacers are widely applied to provide structural support in reverse osmosis and nanofiltration membrane elements to produce high-quality water. However, the spacer poses a challenge for OCT imaging because the spacer material can be (partly) transparent, making it difficult to detect and possibly mistaken for fouling, and the longer optical pathway through the spacer material distorts the image below the spacer. Several studies developed methods to remove the spacer signals from OCT images [3-5]. In this study we build on these methods by including a spacer geometry which has important advantages for i) visualization of the fouling location, ii) selection of datasets relative to the spacer position using a spacer-based coordinate system, and iii) application of feed channel geometry in CFD studies [6]. Visualization of fouling with respect to the feed spacer is important as fouling around the feed spacer strongly impacts operational performance [7]. This study presents a method to overlay a spacer template from CT imaging with the feed spacer in 3D OCT images, more information on the application of the method may be found in the related research article [6]. An algorithm was developed in MATLAB (release 2021b) programming language which uses the following toolboxes: Antenna Toolbox, Computer Vision Toolbox, Curve Fitting Toolbox, Deep Learning HDL Toolbox, Image Processing Toolbox, Optimization Toolbox, Parallel Computing Toolbox, Signal Processing Toolbox, Statistics and Machine Learning, and System Identification Toolbox. The program could be ported to open-source alternatives (e.g., Python) and does not strictly require functions that are exclusive to MATLAB. The workflow consists of three main steps: i) construction of the spacer template from a CT scan, ii) removing background noise and reducing the image file size of a 3D OCT scan, and iii) combining the OCT image with the spacer template. Two MATLAB programs are provided in the supplementary materials together with the necessary functions to run the programs. The program *a_SpacerDemo* generates a spacer template of arbitrary size and rotation from a CT scan of a reference feed spacer. The program *b_Demonstration* generates a specific slice relative to the spacer cell from the combined dataset of the spacer template and the 3D OCT image. The MATLAB programs can be a useful tool in membrane research and may be tailored to the needs of the user.

Construction of the spacer template from a CT scan

The construction of the feed spacer template consisted of the following steps (Fig. 1): First, a computed tomography (CT) scan of a clean 34 mil feed spacer was made, which was then straightened by removing the tilts and bends. This corrected volumetric data was then converted into a spacer template consisting of one spacer cell. Finally, the spacer template was used as a building block to generate a spacer with a preferred number of spacer cells, size, and orientation. These steps are further detailed in the subsequent sections. In the supplementary information, a template (*ReferenceSpacerS863*) of a 34 mil feed spacer and the MATLAB program (*a_SpacerDemo*) that generates a spacer template can be found. Researchers may purchase a “370″ type membrane element from Dupont (e.g., SW30HRLE-370), to harvest corresponding feed-spacers for CT scanning. While an optimal result could be obtained by post-mortem CT scanning of the actual spacer, in the current study a generic scan was used because the geometry of the spacer was very consistent.

Straightening

During the CT scan acquisition, the spacer sample was resting on one edge only. Consequently, the sample was slightly bent and tilted. However, for the subsequent processing, the spacer volume data is required to be straight and well-aligned. The spacer was straightened by forcing its average z-coordinates to lie in a flat plane. The procedure is discussed below and illustrated in Fig. 2.

The outer edge of the spacer was found by Matlab’s *isosurface* function. The outer surface of the spacer is described as a list of vertices (x_i, y_i, z_i) and a list of faces which refers to triplets of vertices (i_1, i_2, i_3). The vertices are shown as grey dots in Fig. 2a (projected on the xz-plane) and Figure Fig. 2b (projected on the yz-plane). A quadratic function (Eq. 1) was fit through the vertices (with “matrix left-division” Matlab *mldivide* function), where the z-coordinate was expressed as a function of the *x*- and *y*-coordinate. The resulting z-coordinates are shown as black dots in Fig 2.

$$\hat{z}_i(x_i, y_i) = a_1 + a_2 x_i + a_3 y_i + a_4 x_i y_i + a_5 x_i^2 + a_6 y_i^2 \tag{1}$$

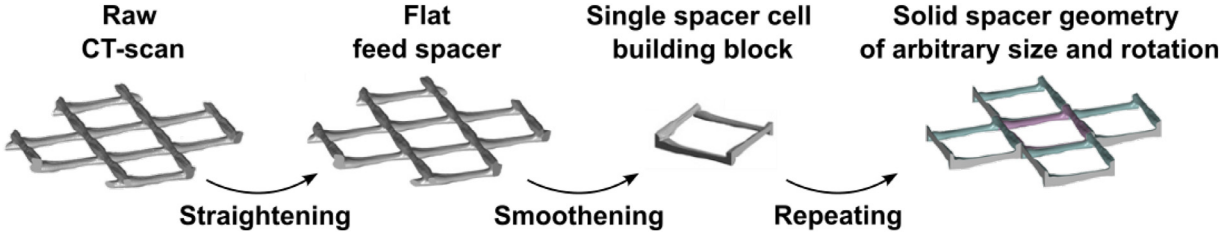

Fig. 1. Summary of the steps taken to obtain the solid spacer geometry from the CT scan of the feed spacer. A 2D spacer template is generated from the solid spacer geometry and will be used to fit the spacer in an OCT image and to correct the distortion of the image below the spacer.

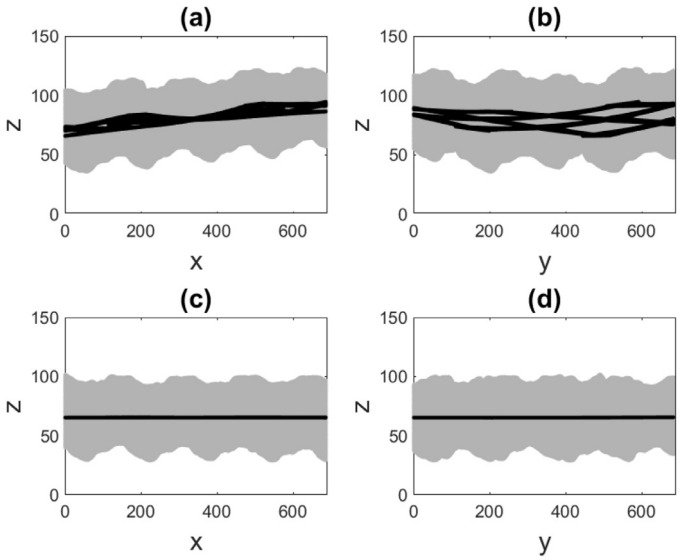

Fig. 2. Straightening of the CT images. The gray dots are all the vertices that describe the surface of the detected spacer. The black dots represent the quadratic surface fitted through the vertices. The spacer is straightened by forcing the 'average' z-coordinate (black dots) in a straight plane. (a) Projection of non-straightened vertices on the x-z plane. (b) Projection of non-straightened vertices on the y-z plane. (c) Projection of straightened vertices corresponding to (a). (d) Projection of straightened points corresponding to (b). In other words, the feed spacer is put in a straight plane.

The resulting surface was made as the average z-coordinate of the edges of the spacer filaments as a function of the x- and y-coordinates. The surface was straightened by correcting the z-coordinates, such that the average z-coordinate would form a straight plane, as shown in Eq. (2). The surface was used for visualization of the feed spacer whereas volumetric data was used for constructing a spacer geometry and further processing. For the volume data, the straightening was done by shifting the data a whole number of voxels and adjusting the number of points in the z-direction accordingly. The maximum correction in the z-direction was 33 voxels, corresponding roughly with a tilt in the x-direction of 20 voxels and a curve in the y-direction of 10 voxels. Compared to the alternative of rotating and bending, it was estimated that an error of ~ 0.04 % was introduced in the length and width coordinates.

$$z_i^c(x_i, y_i) = z_i - \hat{z}_i(x_i, y_i) + \frac{1}{N}\sum_i^N \hat{z}_i(x_i, y_i) \tag{2}$$

The shifted vertices are shown as gray dots in Fig. 2c and d, where the straightened mean z-coordinates are shown as black dots. Fig. 2 demonstrates that the resulting spacer volume data is straight and that even though the resulting spacer shape appears to be regular, minor deviations between individual spacer cells can be seen.

Constructing a single spacer cell building block

To generate a feed spacer geometry of arbitrary size and orientation, it is required to combine individual spacer cells into a larger shape. Spacer cells appear quite similar, nevertheless, small irregularities would result in sharp transitions where individual cells are combined. The straightened volumetric feed spacer data from the CT scan was converted into a single spacer cell building block that can be used to construct smooth and regular solid spacer geometries. This building block was obtained by replacing half of a spacer cell with the moving average of itself and the next spacer cell. This procedure is detailed below and illustrated in Fig. 3.

The straightened spacer volume data was rotated around the z-axis, to align the spacer filaments with the x- and y-coordinates. A rectangular area was selected that corresponds to one spacer cell. This rectangle was placed in a manner that encloses 4 half filaments and the area between them (solid line in Fig. 3). It is worth noting that due to the periodicity of the spacer cells, the location of this rectangle does not have to be precise. The center of this rectangular spacer cell was taken as the reference coordinate (x_0, y_0). A weight factor (w_x) was defined, such that it equals one on the left half of the cell, and linearly decreases to zero in the right half of the cell:

$$w_x(x) = 1 - \frac{x - x_0}{2\Delta x} \; for \; x \geq x_0 \; w_x(x) = 1 \; for \; x < x_0 \tag{3}$$

A new set of volume data (v') was calculated, where the new data was equal to a weighted average of the original data (v) and the original data shifted by one spacer cell (Eq. 4), using the previously defined weight factor (Eq. 3). The left half of the spacer cell was unaffected, whereas the right half of the cell gradually changed into the right half of the cell to the left. This way, it is guaranteed that the left and right edges are identical. The same procedure was also applied in the y-direction.

$$v'(x, y, z) = v(x, y, z)\; w_x(x) \; + v(x - \Delta x, y, z)\big(1 - w_x(x)\big) \tag{4}$$

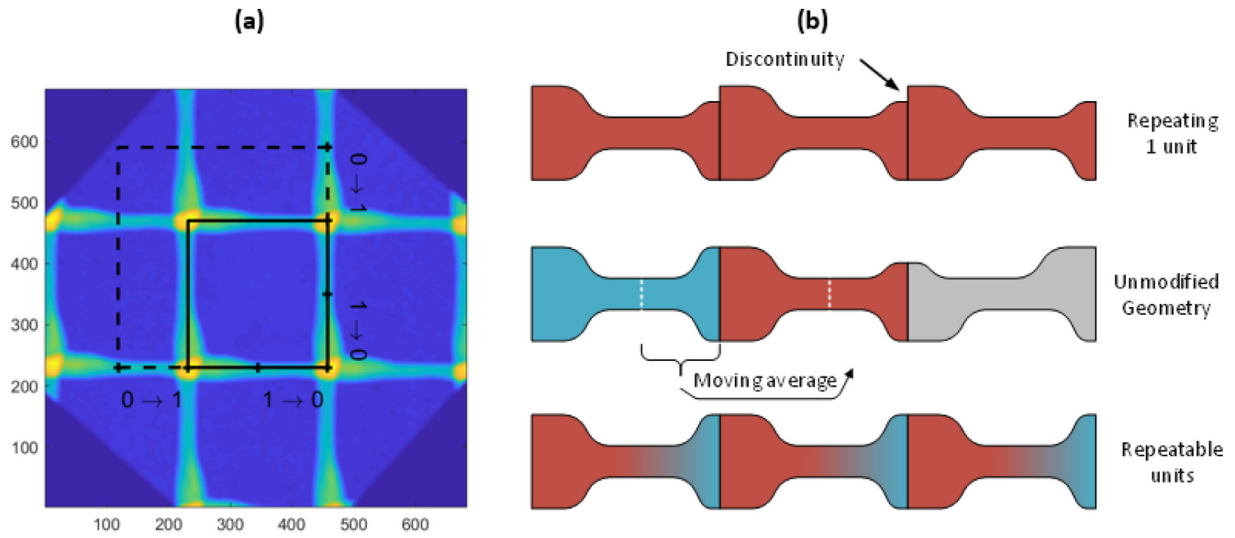

Fig. 3. Constructing a single spacer cell building block. (a) The building block is based on the spacer cell inside of the solid square. (b) The right half of the square is adjusted via a weighted moving average with the spacer cell to the left. Moving to the right the cell gradually changes into the cell to the left. This way, the right and left edges of the cell are identical and transition smoothly. This procedure is repeated for the bottom half of the spacer cell in reference to the spacer cell in (a).

Generating a spacer geometry of arbitrary size and rotation

The single spacer cell building block was used to generate a solid spacer geometry of a certain size and orientation. To this purpose, the coordinates of the OCT data (x_d, y_d) were mapped to the corresponding coordinates of the spacer (x_s, y_s) as illustrated in Fig. 4. This considers that the spacer may be rotated by α and that the center of the cell may be shifted by Δx and Δy. Furthermore, it is

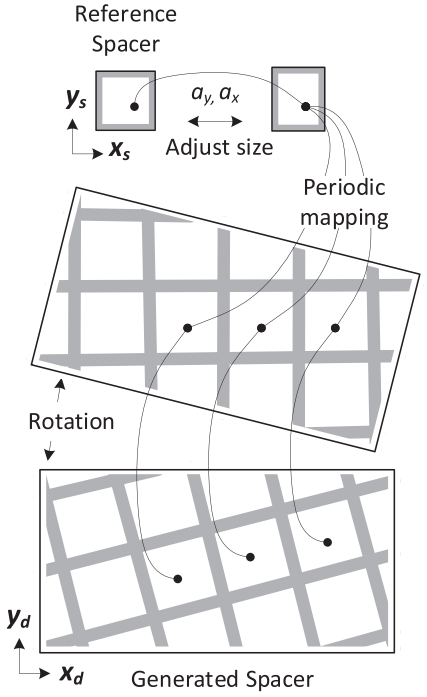

Fig. 4. Generating a solid spacer geometry of arbitrary size and rotation. The size of the reference spacer was adjusted for slight deformations by factors a_x and a_y and the OCT data coordinates (x_d, y_d) were mapped to the corresponding spacer coordinates (x_s, y_s) considering rotation and shift in the x_d and y_d direction.

considered that the spacer may be slightly deformed by a factor a_x and a_y. Since the spacer cells are repeated, the spacer coordinates are modular with the length and width of the spacer cells (a_xL_x, a_yL_y) (Eqs. 5 and 6):

$$x_s = \mathrm{mod}\big(\big(x_d + \Delta x\big)\cos(\alpha) + \big(y_d + \Delta y\big)\sin(\alpha), a_x L_x\big)/a_x \tag{5}$$

and:

$$y_s = \mathrm{mod}\big(-\big(x_d + \Delta x\big)\sin(\alpha) + \big(y_d + \Delta y\big)\cos(\alpha), a_y L_y\big)/a_y \tag{6}$$

The spacer volume data in OCT-image coordinates (v_d) can be found by evaluating the solid spacer geometry volume data (v_s) at the mapped coordinates (Eq. 7). Generally, the coordinates x_s and y_s do not correspond exactly with the coordinates in the solid spacer geometry dataset. This is addressed by interpolation (Matlab's *interp2* function).

$$v_d\big(x_d, y_d, z\big) = v_s\big(x_s, y_s, z\big) \tag{7}$$

Constructing a template for the spacer

A 2D template of the feed spacer was generated from the solid spacer geometry to locate the spacer in an OCT image, and to correct the distortion of the image below the spacer. The shift in the image is proportional to the thickness of the spacer. Thus, a suitable spacer template is a map of the spacer thickness above the membrane (*x,y*-plane), or the sum of the number of voxels in the z-direction that are considered spacer.

Removing background noise and reducing the image file size of an OCT scan

This section describes how the OCT of the spacer-filled channel was obtained. In addition to the acquisition of the raw OCT images, this consisted of determining a correction factor for the length scale in the OCT images and a procedure to smoothen the data.

Estimating background noise

To estimate the mean and variance of the background noise, a histogram of the OCT signal values of all the data points was constructed. The first peak in this histogram is assumed to be formed by the normally distributed background signal. By fitting a Gaussian curve through the first peak, it was possible to obtain an estimate of the mean and variance of the background. Fig. 5 shows a histogram of all the intensity values contained in a 3D OCT scan, the fitted Gaussian curve, and the range where the signal is less than the threshold value. It is necessary that the background noise does not overlap with the signal of the features of interest for

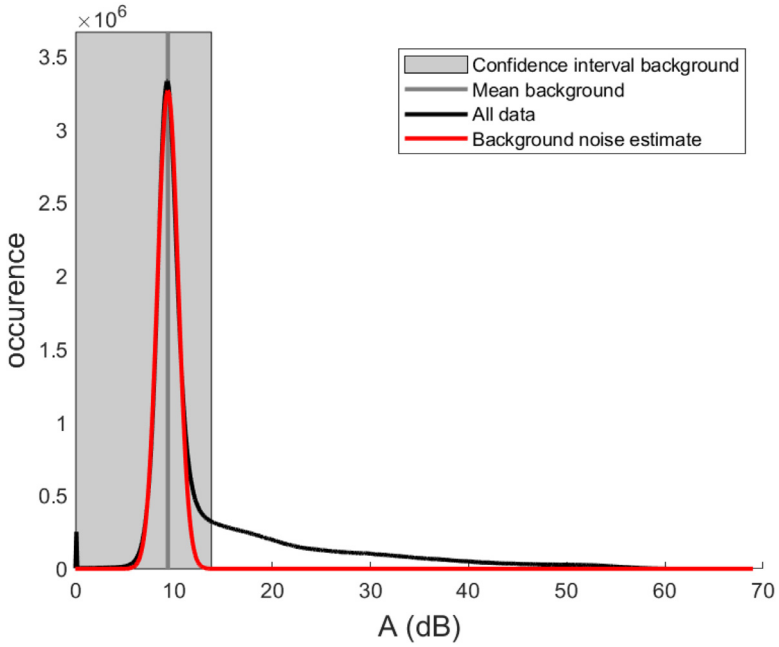

Fig. 5. Histogram of all measured values in a 3D OCT scan. The properties of the background signal are estimated from the largest peak occurring for lower intensity values. This is fit to a Gaussian curve, which yields the mean and variance of the background. The confidence interval for the background is from 0 to mean plus two standard deviations.

visualization and processing. The threshold value (Eq. 8) was defined as the average background plus two standard deviations to effectively separate the noise from the features of interest. With two standard deviations ca. 97.5 % of the background was removed, allowing effectively distinguishing significant features from the background noise.

$$A_{thresh} = \mu_{A,background} + 2\sigma_{A,background} \tag{8}$$

A-scan representation

The theory behind imaging with spectral OCT is well described by Izat and Choma [8]. One consequence of the physical properties of light, mathematical properties of Fourier transforms and the limited wavelength bandwidth of the microscope, is that an ideal reflector does not give a sharp signal, instead, the signal has a Gaussian shape in the z-direction, centered on the location of the reflector. Thus, the signal as relative intensity of an ideal reflector at location $z_{R,}$ with property $I_{R,i}$ may be given by Eq. (9):

$$I_i(z) = I_{R,i} \exp\left(-\left(\frac{z - z_{R,i}}{\Delta z_C}\right)^2\right) \tag{9}$$

Theoretically, Δz_C is the coherence length associated with the properties of the OCT device and applies to its focal plane. However, a larger empirical value may be chosen, to better approximate the properties of the sample and non-ideal properties of the practical system. It is considered that the total measured intensity is the sum of a background (I_0) and the sum of the contributions of all the reflectors Eq. (10):

$$I(z) = I_0 + \sum_i I_{R,i} \exp\left(-\left(\frac{z - z_{R,i}}{\Delta z_C}\right)^2\right) \tag{10}$$

Finally, the signal given by the OCT is the logarithm of the intensity in dB (Eq. 11):

$$A(z) = \frac{1}{10} \log_{10}(I(z)) \tag{11}$$

The concept outlined in (Eqs. 9-11) was used to approximate the raw A-scan data as a list of discrete reflectors. The algorithm identifies the highest intensity value, then places a reflector at that location and subtracts the signal of the new reflector from the raw A-scan value. This process was repeated until there were no more values above the threshold. The result was stored as a list of reflectors ($z_{R,i}$, $I_{R,i}$). The data can be reconstructed by reversing the procedure described above. By reconstructing the data, the data was smoothened in the z-direction, because the variability of the signal below the threshold was discarded by the A-scan approximation procedure.

A-scan approximation

The mean and confidence interval were then used as parameters to approximate the A-scans with a list of discrete reflectors. As example one A-scan is shown in Fig. 6. It can be seen that the features outside of the confidence interval are well approximated and that the smoothened data contains no more background noise.

The approximation of the A-scans by a list of discrete reflectors has two main benefits. Firstly, the required file size is reduced by ca 80 % for data stored as unsigned 8-bit file (e.g. file size is 17 MB for a 3D-scan of 499×499×651). Secondly, the locations of the reflectors can be adjusted without changing the overall dimensions of the scan (Fig. 7).

Combining OCT images with a spacer template

This section describes how the location of the spacer was estimated in an OCT scan. First, a 2D template of the spacer was constructed from the CT scan (see section *Constructing a template for the spacer*), and then a 2D plane of the estimated membrane depth was constructed from the OCT scan. In case no CT scan is available, researchers may construct a 2D template based on an OCT scan of the unfouled membrane and feed spacer. The rotation and shift of the spacer template compared to the membrane location were determined by maximizing the similarity between the template and the estimated membrane depth. Subsequently, the known location of the feed spacer was used to correct for the distortions below the spacer and to select datasets with the same location relative to the position of the spacer. In the supplementary information, the MATLAB program (*b_Demonstration*) that selects a 2D slice with a certain orientation and location compared to the feed spacer from a 3D OCT dataset can be found.

Detecting the membrane

The approximate location of the membrane follows from the known height of the flow channel. Near this point, it was assumed that the location of the maximum signal corresponds to the membrane material. The curvature of the membrane was estimated by fitting a quadratic surface through the membrane height, which was used to correct the curvature of the image. The distortion below the spacer or spacer shadow (M_D) could be found in the 2D array of the estimated membrane depth as the deviation from the average depth and was used later to correlate with the spacer template.

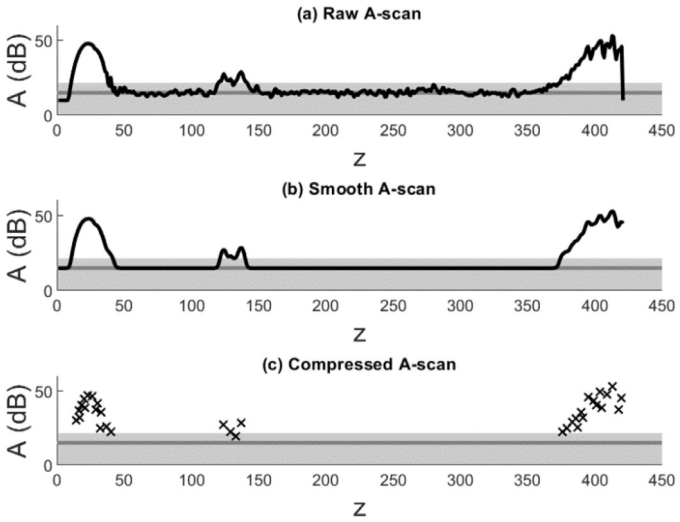

Fig. 6. Comparing the raw A-scan data (a) with the smooth A-scan data (b) and the compressed A-scan data (c). The smooth A-scan is obtained by approximating the data by a sum of discrete reflectors. The compressed data contains only information about the discrete reflectors. The data can be reconstructed by reversing the procedure outlined in Eqs. (9-11) in section *A-scan representation.* The gray line corresponds to the mean of the background and the gray area corresponds to the confidence interval around the background, as determined in Fig. 5. The data points out of the background noise are well approximated by the smoothened data.

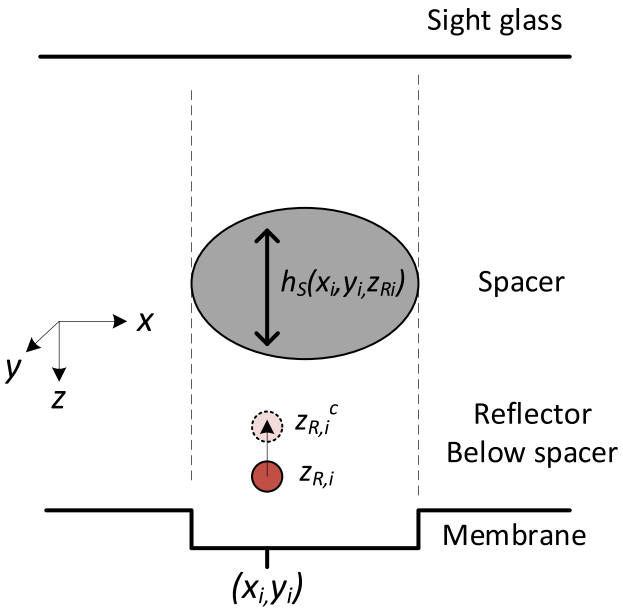

Fig. 7. Correcting for the spacer shadow and the membrane shift. The initial location (Z_R) of each reflector below spacer material was shifted to the actual location (Z_{Rc}) depending on the height of the spacer material (h_s) above it and the relative difference in refractive index between the spacer material and water.

Estimating the spacer location

The spacer location was estimated by matching the spacer shadow (M_D), and the spacer template (M_S). This was achieved by rotating and translating the spacer template and calculating the value of a *cost* function at the applied rotation and translation. The *cost* function (C) is defined based on the correlation between the shadow and the template (Matlab's *corr2* function). Note that the *cost* function is defined in a way that minimizing the *cost* function will maximize the correlation (Eq. 12):

$$C = -corr(M_S, M_D) \tag{12}$$

First, an initial estimate for the translation in *x*- and *y*- direction was obtained by calculating the objective function on a crude grid. For the initial guess, the user-defined rotation is used, because the rotation of the spacer is virtually the same everywhere in the flow cell and can be estimated and controlled relatively more precisely than location. These estimated coordinates and the estimated angle are used as initial values for an optimization procedure (Matlab's *fmincon* function), to refine the translation and rotation of the spacer template.

Correcting for spacer shadow and membrane shift

This section describes how the estimated spacer location may be used to correct the effect of the spacer shadow. The spacer material has a higher refractive index than water, which increases the length of the optical pathway of light passing through spacer filaments. Consequently, features below the spacer appear to be shifted. This is particularly obvious for the membrane, which should be a flat surface.

For each reflector that shares both *x*-and *y*-coordinates with the spacer, the height of the spacer above it (h_s) was determined from the spacer template, and its location was shifted according to the relative difference in refractive index between the spacer material (n_s) and water (n_w) (Fig. 7). The refractive index of the spacer material could be inferred from the thickness of the spacer material and the difference in optical pathway between the spacer and the water in an OCT image of the clean feed channel.

$$z_{R,i}^{C} = z_{R,i} - h_S\left(x_i, y_i, z_{R,i}\right)\frac{n_S - n_W}{n_W} \tag{13}$$

The apparent bending of the membrane was corrected, by fitting the estimated membrane location to a quadratic surface and adjusting the z-coordinates of reflectors accordingly (Eq. 13). In addition, the average membrane location ($\hat{z}_M$) was compared to the known channel depth (h), to estimate the location of the opposite flow-channel boundary (glass) (Eq. 14).

$$z_{R,i}^{C} = z_{R,i} + h - \hat{z}_M\left(x_i, y_i\right) \tag{14}$$

Note that different versions of the data can be obtained by selecting which of the corrections above will be applied. After applying the corrections, the modified volume data for the OCT was reconstructed by reversing the procedure outlined in section *A-scan representation*.

Comparison with alternative protocols for OCT visualization of feed spacer filled channels

The presented automated algorithm for processing OCT images of feed spacer filled channels builds further on existing protocols in three aspects: positioning, correcting, and visualizing. This section compares the presented method with existing methods based on those three aspects.

Some previous studies that observed a single location within a single flow cell did not need to reorient the OCT probe and hence could isolate fouling voxels by background subtraction using an image of the clean feed channel [3,9]. Experiments often include parallel fouling tests involving multiple flow cells, necessitating repositioning of the OCT probe between flow cells. Manual repositioning results in a shift in the x-, y-, and z-direction of the membrane and spacer in an image, which hinders background subtraction. The shift in the z-direction can be overcome by signal intensity-based detection of the membrane location [10]. This was also applied in the current study to detect the membrane and correct the image curvature. Alternatively, state-of-the-art robotic arms have been programmed to move the OCT probe with an accuracy in the range of 8 μm [11-13]. Robotic arms enable repositioning of the OCT probe with respect to a flow cell, but not with respect to a feed spacer cell because the spacer is positioned slightly differently in each experiment. The method presented in this study enables selection of 3D OCT datasets with identical positions with respect to the feed spacer cell. This enables systematic comparison of fouling in parallel tests in spacer filled channels.

The method presented in this work corrects the spacer shadow and the apparent bending of the membrane. Because of the spacer shadow, the feed spacer and image below are often avoided in OCT imaging and image processing [14,15]. Limited previous studies did correct the curvature of the image [16], however to the best of the author's knowledge this study is the first to correct for the spacer shadow and apparent bending of the membrane.

The presented method for combining OCT images of spacer filled channels with a CT scan of the feed spacer is the first of its kind. Previous work either avoided the feed spacer [15,17,18], excluded it in image analysis [14], or presented images in which the spacer geometry was not clearly visible [3,4]. The current method for visualization of fouling with respect to the feed spacer enables the scientific field to finally evaluate the impact of fouling on feed spacers.

Conclusions

In this study, a MATLAB program is presented for analysis of fouling in spacer-filled membrane filtration channels. The program effectively reduces noise and the OCT scan size and adds a feed spacer geometry from a CT scan to the OCT image. The resulting dataset enables improved 3D visualization, selection of datasets relative to the spacer position, and subtraction of the feed channel geometry for application in CFD studies. The developed MATLAB program is automated, allowing the processing of many OCT scans. This feature is advantageous considering that a thorough experimental approach where different locations in multiple parallel test cells are monitored may generate dozens of OCT scans. Finally, the presented method can be a useful tool in membrane research and may be customized to the needs of the user.

Declaration of competing interest

The authors declare that they have no known competing financial interests or personal relationships that could have appeared to influence the work reported in this paper.

CRediT authorship contribution statement

Kees Theo Huisman: Conceptualization, Methodology, Software, Investigation, Writing – original draft. **Luca Fortunato:** Conceptualization, Methodology, Writing – review & editing. **Johannes S. Vrouwenvelder:** Conceptualization, Methodology, Writing – review & editing, Supervision. **Bastiaan Blankert:** Conceptualization, Methodology, Software, Investigation, Writing – review & editing, Supervision.

Data availability

Data will be made available on request.

Acknowledgments

We thank Ran Tao, Matthieu Mulle, and Gilles Lubineau for providing the CT scan of the spacer. This publication is based upon work supported by the King Abdullah University of Science and Technology (KAUST) under Award No. IED OSR-2019–4455.

Supplementary materials

Supplementary material associated with this article can be found, in the online version, at doi:10.1016/j.mex.2024.102871.

References

[1] M. Wagner, H. Horn, Optical coherence tomography in biofilm research: a comprehensive review, 114(7) (2017) 1386–1402. https://doi.org/10.1002/bit.26283.
[2] L. Fortunato, T. Leiknes, In-situ biofouling assessment in spacer filled channels using optical coherence tomography (OCT): 3D biofilm thickness mapping, Bioresour. Technol. 229 (2017) 231–235, doi:10.1016/j.biortech.2017.01.021.
[3] S. West, M. Wagner, C. Engelke, H. Horn, Optical coherence tomography for the in situ three-dimensional visualization and quantification of feed spacer channel fouling in reverse osmosis membrane modules, J. Memb. Sci. 498 (2016) 345–352, doi:10.1016/j.memsci.2015.09.047.
[4] L. Fortunato, S. Bucs, R.V. Linares, C. Cali, J.S. Vrouwenvelder, T. Leiknes, Spatially-resolved in-situ quantification of biofouling using optical coherence tomography (OCT) and 3D image analysis in a spacer filled channel, J. Memb. Sci. 524 (2017) 673–681, doi:10.1016/j.memsci.2016.11.052.
[5] K.T. Huisman, B. Blankert, H. Horn, M. Wagner, J.S. Vrouwenvelder, S. Bucs, L. Fortunato, Noninvasive monitoring of fouling in membrane processes by optical coherence tomography: a review, J. Memb. Sci. 692 (2024) 122291, doi:10.1016/j.memsci.2023.122291.
[6] K.T. Huisman, L. Fortunato, J.S. Vrouwenvelder, B. Blankert, A clear view of biofouling in spacer filled membrane filtration channels: integrating OCT and CT for improved visualization and localization, J. Memb. Sci. 697 (2024) 122573, doi:10.1016/j.memsci.2024.122573.
[7] K.T. Huisman, N. Franco-Clavijo, J.S. Vrouwenvelder, B. Blankert, Improved quantitative evaluation of the fouling potential in spacer-filled membrane filtration channels through a biofouling index based on the relative pressure drop, J. Memb. Sci. 671 (2023) 121400, doi:10.1016/j.memsci.2023.121400.
[8] J.A. Izatt, M.A. Choma, Theory of Optical Coherence Tomography, in: W. Drexler, J.G. Fujimoto (Eds.), Optical Coherence Tomography: Technology and Applications, Springer Berlin Heidelberg, Berlin, Heidelberg, 2008, pp. 47–72. https://doi.org/10.1007/978-3-540-77550-8_2.
[9] L. Fortunato, S. Jeong, T. Leiknes, Time-resolved monitoring of biofouling development on a flat sheet membrane using optical coherence tomography, Sci. Rep. 7 (1) (2017) 15, doi:10.1038/s41598-017-00051-9.
[10] W. Li, X. Liu, Y.-N. Wang, T.H. Chong, C.Y. Tang, A.G. Fane, Analyzing the evolution of membrane fouling via a novel method based on 3D optical coherence tomography imaging, Environ. Sci. Technol. 50 (13) (2016) 6930–6939, doi:10.1021/acs.est.6b00418.
[11] L. Fortunato, S. Jeong, Y. Wang, A.R. Behzad, T. Leiknes, Integrated approach to characterize fouling on a flat sheet membrane gravity driven submerged membrane bioreactor, Bioresour. Technol. 222 (2016) 335–343, doi:10.1016/j.biortech.2016.09.127.
[12] A. Depetris, A. Wiedmer, M. Wagner, S. Schäfer, T.J. Battin, H. Peter, Automated 3d optical coherence tomography to elucidate biofilm morphogenesis over large spatial scales, J. Visualized Experim. 2019 (150) (2019), doi:10.3791/59356.
[13] L. Gierl, K. Stoy, A. Faíña, H. Horn, M. Wagner, An open-source robotic platform that enables automated monitoring of replicate biofilm cultivations using optical coherence tomography, npj Biofilms Microbiomes 6 (1) (2020) 18, doi:10.1038/s41522-020-0129-y.
[14] X. Liu, W. Li, T.H. Chong, A.G. Fane, Effects of spacer orientations on the cake formation during membrane fouling: quantitative analysis based on 3D OCT imaging, Water Res. 110 (2017) 1–14, doi:10.1016/j.watres.2016.12.002.
[15] S. Park, Y.D. Jeong, J.H. Lee, J. Kim, K. Jeong, K.H. Cho, 3D printed honeycomb-shaped feed channel spacer for membrane fouling mitigation in nanofiltration, J. Memb. Sci. 620 (2021) 118665, doi:10.1016/j.memsci.2020.118665.
[16] M. Wagner, D. Taherzadeh, C. Haisch, H. Horn, Investigation of the mesoscale structure and volumetric features of biofilms using optical coherence tomography, Biotechnol. Bioeng. 107 (5) (2010) 844–853, doi:10.1002/bit.22864.
[17] J. Yu, D. Chen, J.J. Wu, B. Wang, R.W. Field, Arch-type feed spacer with wide passage node design for spiral-wound membrane filtration with reduced energy cost, Desalination 540 (2022) 115980, doi:10.1016/j.desal.2022.115980.
[18] X. Liu, D. Du, G. Tu, W. Li, Unraveling effects of Dean vortices on membrane fouling in a sinusoidally curved channel, J. Memb. Sci. 603 (2020) 118008, doi:10.1016/j.memsci.2020.118008.